Experimental Determination of Aeroelastic Derivatives for a Small-Scale Bridge Deck

Mario Cassaro, Enrico Cestino, Giacomo Frulla, Pier Marzocca, Mark Pertile

Experimental determination of aeroelastic derivatives for a small-scale bridge deck

M. Cassaro, E. Cestino, G. Frulla, P. Marzocca, M. Pertile

***Abstract*—**A heaving and pitching two degrees of freedom bridge-deck sectional model apparatus representative of a long-span bridge was designed, built, and tested in the wind tunnel to acquire measurement of aeroelastic derivatives. The main objective of this study was the experimental validation of the procedure to compute the aeroelastic derivatives based on the Iterative Least Square Method identification technique. A good correspondence was found between the flutter derivatives experimentally extracted from the model, and the corresponding reference values, which have been analytically derived from the Theodorsen's theory. A simulation model in MATLAB/Simulink® environment, useful for future control laws applications, was also developed and validated by real experimental results.

***Keywords*—**Aeroelastic derivatives identification, small-scale bridge model, wind tunnel experiments.

I. Introduction

AEROELASTICITY is the subject that describes the interaction of aerodynamic, inertia and elastic forces on a flexible structure and the phenomena that can result. It is not only concerned with aircraft but this topic is relevant for the design of structures such as bridges, F1 racing car, turbomachinery blades, wind turbine, helicopters, etc. Aeroelastic phenomena can be either static, the one dealing with non-oscillatory effects of aerodynamic forces acting on a flexible structure (e.g. aeroelastic static stability, inversion of control, divergence), or dynamic, considering the oscillatory effects of the aeroelastic interaction (e.g. galloping, vortex-shedding, buffet, flutter), ([1],[2]). Flutter is a major dynamic aeroelastic problem; it interests lifting surfaces and the occurrence is due to the coupling of vibrational modes of different degrees of freedom of the structure, classical flutter for example involves the coupling of flexural bending and torsional modes. In correspondence of the critical speed and critical frequency, the unsteady aerodynamic forces produced by the oscillation of the structure are such that self-sustained motion occurs. Above the critical speed of flutter, the oscillations increase in amplitude with remarkable rapidity and catastrophic effects on the structure might occur. Long span structures in general might be affected by this phenomenon and their torsional stiffness and mass distribution are such that inertial coupling between bending (either edgewise or flapwise) and torsion modes is triggered.

In the present day, the design and analysis of long-span bridges entails, among others, a proper assessment of the flow-structure interactions occurring when the bridge is exposed to wind loading. Before the Tacoma Narrows bridge failure in 1940, long-span bridges were predominantly designed for static wind loads only. Such unexpected collapse clearly demonstrated the need of considering dynamic aerodynamic loading and the aeroelastic behavior of a bridge deck in the design synthesis of these long-span structures.

Very long-span bridges have a remarkable low natural frequencies and the ratio between the fundamental torsional and vertical mode frequencies is also quite low. This renders long spans bridges, examples provided in Figure 1, very susceptible to the actions of strong winds, which can trigger fatiguing vortex-induced vibration and turbulence-induced buffeting and catastrophic flutter instability. The 1998 Akashi Kaikyõ Bridge (Japan), with a main span of 1991 m, is the world longest cable-stayed bridge. However we do not need to reach to these spans to perceive flow-structure interaction to be problematic. Indeed, the Tatara Bridge (Japan), with a main span of 890 m, has already indicated the significance of including aerodynamic and aeroelastic design practices in long-spans bridge construction. Advanced understanding of the wind-bridge interaction are necessary to satisfy the increasing needs of safety, reliability, maintainability and budget constraints. In the last fifteen years several long-span bridges were built and the length of the main bridge span has increased since, often requiring appropriate engineering studies of stability and reliability. Without any doubt, the effect of wind on the bridge-deck is a primary concern of bridge designers, as demonstrated by the rich literature on the topic ([3], [4], [5,6], [7],[8]). Details pertaining to several aeroelastic derivatives identification procedures are discussed in [3] and not reported here for sake of brevity. Amongst the different methodologies available, the Iterative Least Square

This work was supported in part by the US National Science Foundation (NSF), Grant under grant no. NSF-CMMI-1031036 and in part by European Commission under Grant n. 269160 FP7-PEOPLE-2010-IRSES, Advanced Aircraft Network for Theoretical & Experimental Aeroservoelastic Modeling.

G. Frulla is with Politecnico di Torino DIMEAS Corso Duca degli Abruzzi 24,10129,Torino,Italy (corresponding author phone: +390110906842; fax: +390110906999; e-mail: giacomo.frulla@polito.it).

E. Cestino is with Politecnico di Torino DIMEAS Corso Duca degli Abruzzi 24,10129,Torino,Italy.(phone:+390110906818;fax: +390110906999; e-mail: enrico.cestino@polito.it).

M. Cassaro is with Département Traitement de l'Information et Systèmes, ONERA, Toulouse, France.

P. Marzocca is with School of Engineering, Aerospace Engineering and Aviation, Royal Melbourne Institute of Technology, Australia.

M. Pertile is with COVAL Italia S.r.l , 10098, Rivoli (TO).

Method, ILMS, is chosen and applied to the case in hand. The reasons rely in its relative implementation simplicity and accuracy but most importantly for the possibility of easily being extended to the full motion 3D-18 derivatives experimental case.

The frequency-domain approach has been widely used for estimating flutter speed of structures ([4]). The frequency-domain method uses flutter derivatives, which may be slender and flexible designs requires improved aeroelastic models along with experimental tests which will give the opportunity to modify and calibrate theoretical models, with the main goal of showing the effect of theoretical approximation and their limits, especially when various sources of uncertainty (loads, structure, material and technological processes) have to be taken into consideration ([15, 16, 17]). Aeroelastic coupling and flexible structures

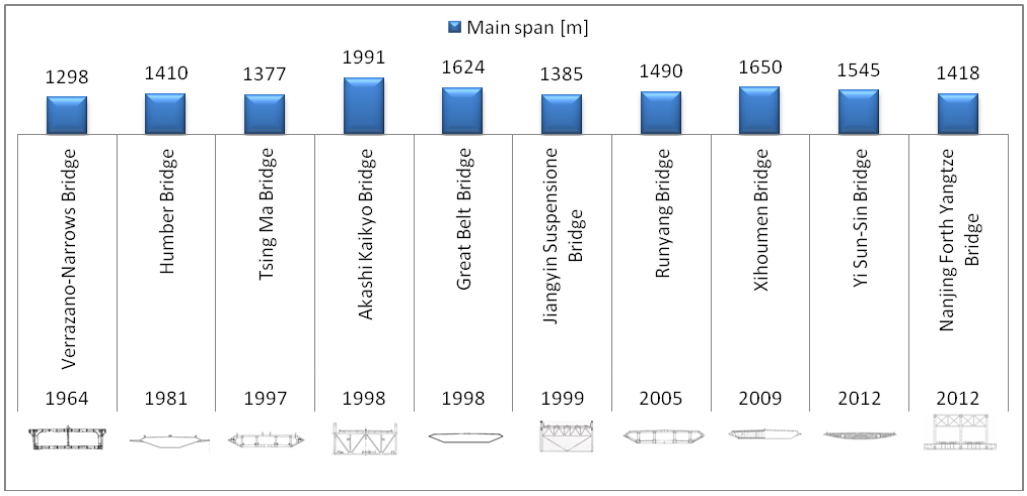

Figure 1 Evolution in time of long spans bridges

experimentally obtained from wind tunnel testing of section models. Extraction of flutter derivatives can be done through the forced vibration technique or the free vibration technique. A method to identify flutter derivatives of bridge decks is developed by ([9]). The flutter derivatives of the Jiangyin Bridge over Yangtze River with a main span of 1385 was used to validate their procedure and results shows a good agreement compared with that from full bridge aeroelastic model wind tunnel test. The ILS methods was used in ([10]) to extract all 18 flutter derivatives for an NACA 0020 airfoil section model demonstrating the accuracy of the procedure by comparing the results obtained from all possible DOF combinations. A recent experimental setup for the extraction of flutter derivatives was built and employed at Clarkson University (USA) as part of two different projects. The first project was funded by NSF (National Science Foundation) under grant no. NSF-CMMI-1031036 and had the focus of developing and applying Reduced Order Models to investigate wind-induced bridge-structures vibrations and enhance understanding of fluid-structure interactions, ([11, 12, 13, 14]). A second project funded by EU under the FP7 Marie Curie actions (A2-NET-TEAM Project no. 269160) was also carried out where the objective was to build a multi-disciplinary network of researchers with complementary expertise to study the aeroelastic behavior of next generation light weight slender structures like innovative next generation aircrafts and High Altitude Long Endurance (HALE) UAVs.

The implementation of new, lightweight composites in behavior have been under investigation by authors in order to explore the potential for energy harvesting from oscillating structures . Some preliminary results are presented in [18,19,20,21]. The detailed simulation of aeroelastic system is fundamental for such specific future configurations.

In particular, in order to investigate the behavior of the system in the post-critical condition, it will be necessary to modify the aerodynamic model introducing nonlinearities due to the dynamic stall [22] and the structural model to introduce possible geometrical nonlinearities [23, 24].

The main objectives of the present research are to 1) validate the experimental procedure to extract flutter derivatives from a scaled model and 2) to demonstrate the improved accuracy in simulation when experimental based derivatives are employed instead of the theoretical values counterparts. Flutter derivatives are dimensionless functions of the reduced frequency and represent the derivatives of the aerodynamic coefficients with respect the displacement functions and their velocity, therefore considering a state of motion, and not in static conditions In this respect, wind tunnel experimental investigations were performed using the Great Belt Bridge (Denmark) cross-section bridge deck model to study the aeroelastic dynamic behavior of a section of a bridge in response to the wind loading, to extract the aerodynamic derivatives and to analyze the flutter aeroelastic instability behavior. Furthermore, to contextualize the experimental campaign and assert the validity of the proposed approach, an appropriate analytical aeroelastic model based on the

Theodorsen's theory is proposed and used in order to obtain the aeroelastic theoretical coefficients.

Using a two Degrees-of-Freedom (DOF) system is possible to obtain eight different flutter derivatives, respectively, four of these are related to plunge motion and four are related to the torsional motion. In this study, following the procedure utilized by Chowdhury & Sarkar [10], a new system identification technique (Iterative Least Square Method – ILSM) is used to identify the values of the flutter derivatives. The ILSM system identification is carried out by means of numerical simulations performed in Matlab® where a non-linear regression tools is applied to the free vibration time histories obtained from the wind tunnel experimental measurements ([25]). The technique is applied to both a 1-DOF system, which is simpler to analyze when only torsional derivatives are concerned, and a 2-DOF plunging and pitching system to obtain the entire set of aeroelastic derivatives. Consistency between the two tests' results in torsion is also used to validate the procedure.

Aeroelastic derivatives are validated by implementing them into a simulation environment correctly describing the dynamic response of the bridge. Although not within the scope of this paper, it is worth noting that the simulation environment was developed to explore the application of robust and adaptive algorithm ([26]) for active aeroelastic vibration suppression.

The rest of the paper is organized as follow: in Section 2 the mathematical model of a 2 DOF wing section is presented; Section 3 describes the experimental setup and the employed procedure to extract flutter derivatives; In Section 4, comparative analysis between the theoretical and experimental results is carried out and presented, together with the simulation response obtained; Section 5 concludes the paper with comments and final discussion.

II. Mathematical Model

Forces arising from the fluid-structure interaction can be described by unsteady aerodynamic models; one of these models describes the 2-D flow as incompressible and fully attached. Thin airfoil theory can be used in first instance as a crude approximation to model the aerodynamic loads on the bridge-deck specifically when its cross-section resembles a thin lifting surface. Even if such simple model cannot be applied directly to study the full aeroelastic behavior of a bluff body under unsteady loads, which often requires knowledge of the viscous effect including flow separation and wake effect, it does describes satisfactorily the forces acting on a bridge-deck. For this reason the unsteady aerodynamic forces are calculated in first approximation using the linearized Theodorsen's approach ([27,28]) and the subsequent flutter analysis will be conducted based on his approach. Theodorsen's theory assumes a thin airfoil is oscillating about the shear center and unsteady loading is composed of two components:

• non-circulatory component, which is not related to vorticity and is correlated to the 'Apparent inertia forces', i.e. mass of air accelerates with the airfoil and introduces a reactive force and moment upon the airfoil.

• circulatory component, which is related to the vortex sheet on the body and in the wake.

The equations of motion in terms of aeroelastic coefficients can be expressed as ([1], [27],[6]):

$$\begin{bmatrix} 1 & x_\alpha \\ x_\alpha & 1 \end{bmatrix} \begin{Bmatrix} \ddot{h} \\ \ddot{\alpha} \end{Bmatrix} + \begin{bmatrix} 2\varsigma_h\omega_h & 0 \\ 0 & 2\varsigma_\alpha\omega_\alpha \end{bmatrix} \begin{Bmatrix} \dot{h} \\ \dot{\alpha} \end{Bmatrix} + \begin{bmatrix} \omega_h^2 & 0 \\ 0 & \omega_\alpha^2 \end{bmatrix} \begin{Bmatrix} h \\ \alpha \end{Bmatrix} = \begin{Bmatrix} -L/m \\ M/I_\alpha \end{Bmatrix} \quad (1)$$

where:

$$2\varsigma_h\omega_h = \frac{c_h}{m} \qquad \omega_h^2 = \frac{K_h}{m}$$

$$2\varsigma_\alpha\omega_\alpha = \frac{c_\alpha}{I_\alpha} \qquad \omega_\alpha^2 = \frac{K_\alpha}{I_\alpha}$$

and ω_h, ω_α [rad/s] are the natural frequencies of the undamped oscillations; ζ_h,ζ_α are the system natural damping of the system; m [Kg/m] is the total mass of the system per unit of length; [Kg·m] is the moment of inertia about the elastic axis of the section, per unit of length; and x_α [m] is the distance between the elastic axis and the center of gravity, see Figure 2. Considering the thin-airfoil theory, the lift (z-axis positive downward) and aerodynamic moment (positive nose-up) about the shear center, expressed per unit span, combining circulatory and non-circulatory components and considering an oscillatory harmonic motion, can be cast as ([1]):

$$L = \left\{\pi\rho b^2\left(-\omega^2 h_0 + i\omega V_\infty \alpha_0 + \omega^2 ba\alpha_0\right)\right\} e^{i\omega t} + \\ + \left\{2\pi\rho V_\infty b\left[F(k) + iG(k)\right]\left[i\omega h_0 + V_\infty\alpha_0 + i\omega b\left(\frac{1}{2} - a\right)\alpha_0\right]\right\} e^{i\omega t} \quad (2)$$

$$M = \left\{\pi\rho b^2\left[-\omega^2 ba h_0 - i\omega V_\infty b\left(\frac{1}{2} - a\right)\alpha_0 + \omega^2 b^2\left(\frac{1}{8} + a^2\right)\alpha_0\right]\right\} e^{i\omega t} + \quad (3) \\ + \left\{2\pi\rho V_\infty b^2\left(a + \frac{1}{2}\right)\left[F(k) + iG(k)\right]\left[i\omega h_0 + V_\infty\alpha_0 + i\omega b\left(\frac{1}{2} - a\right)\alpha_0\right]\right\} e^{i\omega t}$$

Equations (2) and (3) can be expressed in terms of the dimensionless flutter derivatives as follows:

$$L = 2q_\infty b\left(kH_1^*\frac{\dot{h}}{V_\infty} + kH_2^*\frac{\dot{\alpha}b}{V_\infty} + k^2H_3^*\alpha + k^2H_4^*\frac{h}{b}\right) \quad (4)$$

$$M = 2q_\infty b^2\left(kA_1^*\frac{\dot{h}}{V_\infty} + kA_2^*\frac{\dot{\alpha}b}{V_\infty} + k^2A_3^*\alpha + k^2A_4^*\frac{h}{b}\right) \quad (5)$$

where $q_\infty = \frac{1}{2}\rho V_\infty^{\,2}$ is the dynamic pressure, [kg/m^3] is the air density, b [m] is the semi-chord, s [m] is the deck section span, k=(ω_f b)/V_∞ is the reduced frequency and $H_1^*, H_2^*, H_3^*, H_4^*, A_1^*, A_2^*, A_3^*, A_4^*$ are the dimensionless flutter derivatives. Developing (2) and (3) and comparing it with the equations in terms of flutter derivatives (4), (5), it is possible to identify the formulations of the flutter derivatives in terms of Theodorsen's function:

$$H_1^* = \frac{2\pi F}{k} \qquad H_2^* = \frac{2\pi\left[\frac{1}{2} + F\left(\frac{1}{2} - x_\alpha\right) + \frac{G}{k}\right]}{k}$$

$$H_3^* = \frac{2\pi\left[\frac{x_\alpha k^2}{2} + F - kG\left(\frac{1}{2} - x_\alpha\right)\right]}{k^2} \qquad H_4^* = -\frac{\pi k^2 + 2\pi G k}{k^2}$$

$$A_1^* = \frac{2\pi\left[F\left(\frac{1}{2} - x_\alpha\right)\right]}{k}$$

$$A_2^* = \frac{2\pi\left[-\frac{1}{2}\left(\frac{1}{2} - x_\theta\right) - F\left(x_\alpha^2 - \frac{1}{4}\right) + \frac{G}{k}\left(\frac{1}{2} + x_\alpha\right)\right]}{k}$$

$$A_3^* = \frac{\pi\left[k^2\left(\frac{1}{8} + x_\alpha^2\right) + 2F\left(x_\alpha + \frac{1}{2}\right) + 2kG\left(x_\alpha^2 - \frac{1}{4}\right)\right]}{k^2}$$

$$A_4^* = -\frac{2\pi\left[\frac{ak^2}{2} + k\left(x_\alpha + \frac{1}{2}\right)G\right]}{k^2}$$

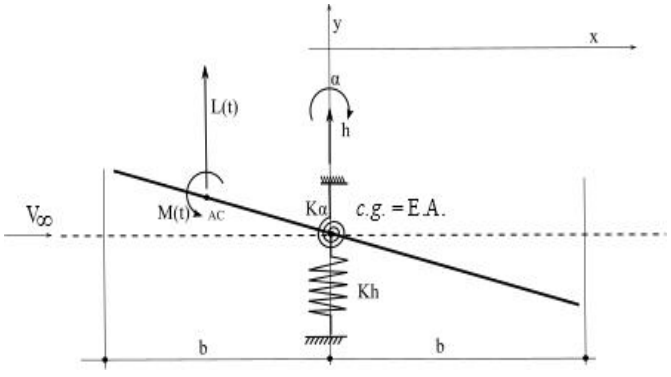

Figure 2 2D Aeroelastic reference section

where F and G are respectively the real and the imaginary parts of the Theodorsen's function. The system of equation presented in equation (1) can be expressed as a state-space formulation: $\{\dot{x}\} = [A]\{x\}$ where $\{\dot{x}\}, \{x\}$ are the state vectors and $[A]$ is the state matrix. Equations (4) and (5) can then be re-written in a form suitable for the state-space formulation, by obtaining the aerodynamic contribution in terms of states acceleration, $\ddot{h}$ and $\ddot{\alpha}$, as follows:

$$\frac{L}{m} = \frac{2q_\infty bs}{m}\left[\frac{kH_1^*}{V_\infty}(\dot{h}) + \frac{bkH_2^*}{V_\infty}(\dot{\alpha}) + \frac{k^2H_4^*}{b}(h) + k^2H_3^*(\alpha)\right] \quad (6)$$

$$\frac{M}{I_\alpha} = \frac{2q_\infty b^2 s}{I_\alpha}\left[\frac{kA_1^*}{V_\infty}(\dot{h}) + \frac{bkA_2^*}{V_\infty}(\dot{\alpha}) + \frac{k^2A_4^*}{b}(h) + k^2A_3^*(\alpha)\right] \quad (7)$$

Herein, m is the mass of the entire system, I_α the moment of inertia about the elastic axis and s the span of the analyzed section.

Considering the aeroelastic equations of motion (1), the state matrix of the state-space formulation, contains terms due to the damping matrix plus the aerodynamic contributes and terms due to the stiffness matrix plus the aerodynamic contributes. The mass, damping, and stiffness matrix in the case of $x_\alpha = 0$ are defined as follows:

$$[M] = \begin{bmatrix} 1 & 0 \\ 0 & 1 \end{bmatrix}; \; [C] = \begin{bmatrix} 2\zeta_h\omega_h & 0 \\ 0 & 2\zeta_\alpha\omega_\alpha \end{bmatrix}; \; [K] = \begin{bmatrix} \omega_h^2 & 0 \\ 0 & \omega_\alpha^2 \end{bmatrix} \quad (8)$$

With this assumption the state-space formulation of the system become:

$$\begin{Bmatrix} \ddot{h} \\ \ddot{\alpha} \\ \dot{h} \\ \dot{\alpha} \end{Bmatrix} = \begin{bmatrix} -2\zeta_h\omega_h & 0 & -\omega_h^2 & 0 \\ 0 & -2\zeta_\alpha\omega_\alpha & 0 & -\omega_\alpha^2 \\ 1 & 0 & 0 & 0 \\ 0 & 1 & 0 & 0 \end{bmatrix} \begin{Bmatrix} \dot{h} \\ \dot{\alpha} \\ h \\ \alpha \end{Bmatrix} + \begin{Bmatrix} -L/m \\ M/I_\alpha \\ 0 \\ 0 \end{Bmatrix} \quad (9)$$

Finally, considering the expressions of lift and moments, Eqs. (6) and (7), in terms of state-space formulation one obtains the following form:

$$\begin{Bmatrix} \ddot{h} \\ \ddot{\alpha} \\ \dot{h} \\ \dot{\alpha} \end{Bmatrix} = \begin{bmatrix} [A1] & [A2] \\ [A3] & [A4] \end{bmatrix} \begin{Bmatrix} \dot{h} \\ \dot{\alpha} \\ h \\ \alpha \end{Bmatrix} \quad (10)$$

$$[A1]=\begin{bmatrix} -2\varsigma_h\omega_h-\dfrac{2q_\infty bskH_1^*}{mV_\infty} & -\dfrac{2q_\infty b^2skH_2^*}{mV_\infty} \\ \dfrac{2q_\infty b^2skA_1^*}{I_\alpha V_\infty} & -2\varsigma_\alpha\omega_\alpha+\dfrac{2q_\infty b^3skA_2^*}{I_\alpha V_\infty} \end{bmatrix}$$

$$[A2]=\begin{bmatrix} -\omega_h^2-\dfrac{2q_\infty sk^2H_4^*}{m} & -\dfrac{2q_\infty bsk^2H_3^*}{m} \\ \dfrac{2q_\infty bsk^2A_4^*}{I_\alpha} & -\omega_\alpha^2+\dfrac{2q_\infty b^2sk^2A_3^*}{I_\alpha} \end{bmatrix}$$

$$[A3]=\begin{bmatrix} 1 & 0 \\ 0 & 1 \end{bmatrix}$$

$$[A4]=\begin{bmatrix} 0 & 0 \\ 0 & 0 \end{bmatrix}$$

The state matrix $[A]$ is subdivided in two contributions:

1) the mechanical contribution $[A^{mec}]$: corresponding to the damping and stiffness matrix due only to the mechanical system and not influenced by the presence of the airflow $(V_{wind})=0$:

$$[C^{mec}]=\begin{bmatrix} -2\varsigma_h\omega_h & 0 \\ 0 & -2\varsigma_\alpha\omega_\alpha \end{bmatrix} \qquad (11)$$

$$[K^{mec}]=\begin{bmatrix} -\omega_h^2 & 0 \\ 0 & -\omega_\alpha^2 \end{bmatrix}$$

2) the effective contribution $[A^{eff}]$ corresponding to the damping and stiffness matrix influenced by the aerodynamic contribute due to the velocity of the flow $(V_\infty)\neq 0$:

$$[C^{eff}]=\begin{bmatrix} -2\varsigma_h\omega_h-\dfrac{2q_\infty bskH_1^*}{mV_\infty} & -\dfrac{2q_\infty b^2skH_2^*}{mV_\infty} \\ \dfrac{2q_\infty b^2skA_1^*}{I_\alpha V_\infty} & -2\varsigma_\alpha\omega_\alpha+\dfrac{2q_\infty b^3skA_2^*}{I_\alpha V_\infty} \end{bmatrix} \qquad (12a)$$

$$[K^{eff}]=\begin{bmatrix} -\omega_h^2-\dfrac{2q_\infty sk^2H_4^*}{m} & -\dfrac{2q_\infty bsk^2H_3^*}{m} \\ \dfrac{2q_\infty bsk^2A_4^*}{I_\alpha} & -\omega_\alpha^2+\dfrac{2q_\infty b^2sk^2A_3^*}{I_\alpha} \end{bmatrix} \qquad (12b)$$

Considering the expressions of the matrices $[C^{mec}],[K^{mec}],[C^{eff}],[K^{eff}]$, starting from a null velocity of the fluid in the wind tunnel and arising its velocity step by step, it is possible to compute all the terms of the matrices above and, knowing their values and with the comparison of the matrices $[A^{mec}]$ and $[A^{eff}]$, all the eight flutter derivatives in function of the fluid velocity:

$$H_1^*=-\frac{m}{\rho sb^2\omega_f}\left(C_{1,1}^{eff}-C_{1,1}^{mec}\right)$$

$$H_2^*=-\frac{m}{\rho sb^3\omega_f}\left(C_{1,2}^{eff}-C_{1,2}^{mec}\right)$$

$$H_3^*=-\frac{m}{\rho sb^3\omega_f^2}\left(K_{1,2}^{eff}-K_{1,2}^{mec}\right)$$

$$H_4^*=-\frac{m}{\rho sb^2\omega_f^2}\left(K_{1,1}^{eff}-K_{1,1}^{mec}\right)$$

$$A_1^*=\frac{I_\theta}{\rho sb^3\omega_f}\left(C_{2,1}^{eff}-C_{2,1}^{mec}\right)$$

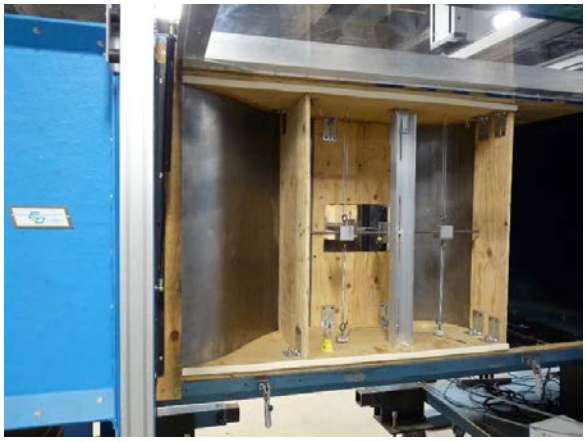

Figure 3 Clarkson University wind tunnel, apparatus mounted inside the test section

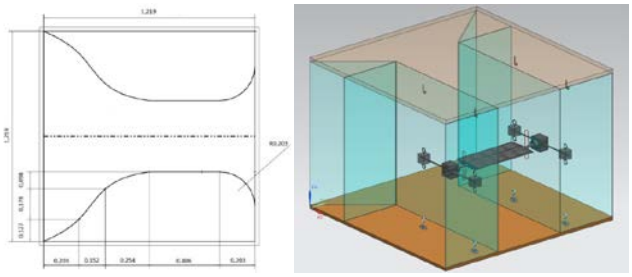

Figure 4 2D heaving-pitching apparatus, schematic and isometric view

$$A_2^*=\frac{I_\theta}{\rho sb^4\omega_f}\left(C_{2,2}^{eff}-C_{2,2}^{mec}\right)$$

$$A_3^*=\frac{I_\theta}{\rho sb^4\omega_f^2}\left(K_{2,2}^{eff}-K_{2,2}^{mec}\right)$$

$$A_4^* = \frac{I_\theta}{\rho s b^3 \omega_f^2}\left(K_{2,1}^{eff} - K_{2,1}^{mec}\right)$$

where ω_f is the flutter frequency [rad/s] which is computed experimentally, and $K_{(...)}^{(...)}$ and $C_{(...)}^{(...)}$ are the coefficients of the stiffness and damping matrices, in condition of 'wind-off' and 'wind-on', respectively.

III. Experimental Tests

Experimental tests were carried out in the Clarkson University Eiffel type subsonic wind tunnel where a rigid section was elastically suspended to simulate the plunging and pitching aeroelastic behavior of a bridge-deck under aerodynamic loading conditions, see Figure 3. The test section measures 1.22 m wide by 0.91 m tall (48x36 in) with a length

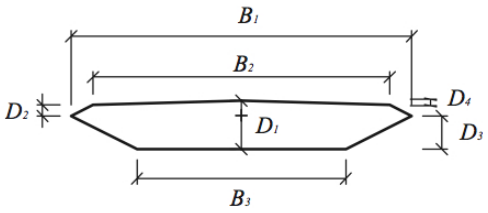

Scale coeff. 1/155	B_1	B_2	B_3	D_1	D_2	D_3	D_4
Full scale [m]	31	27	19	4,4	1	3	0,4
Model [m]	0.2	0.174	0.123	0.028	0.006	0.019	0.003

Model span [m]	Model width [m]	Model depth [m]
0.4	0.2	0.028

Figure 5 Bridge section schematic and dimensions

of 1.52 m (60 in). The diffuser section expands the flow downstream of the test section through a 9 m length (354 in). The tunnel power section, located at the diffuser outlet, is a 2.1 m (84 in) vane-axial fan with 16 adjustable blades. In order to simulate the dynamic behavior of a bridge section, using the Great Belt Bridge, GBB, (Halsskov-Sprogø – Denmark) as cross-section, a complete model apparatus has been developed such that pitching and heaving motion could be monitored and recorded either separately or coupled. The designed and built apparatus, is shown in mounted configuration in Figure 3, and consists of a convergent, reduced test section and a divergent, as shown in Figure 4, restrained by two plywood floors, located at the base and at the top. This choice is due to the reduced dimension of the bridge section model, and the need of installing the required motion and measuring instrumentation. Moreover, the convergent has been designed with a contraction ratio 3:1 to balance the blockage effect of the whole apparatus and, therefore to guarantee the same wind speed performance at the inner test section. This has been experimentally demonstrated by monitoring the wind speed at the inner test section with a pitot probe. The scaled bridge section is made by aluminum and represents a scaled generic section of the real GBB, with scale factor of 1/155 as reported

Figure 6 Top view of the deck section with mechanical link (CAD) and restraining system with C-section bar

Table 1. System's components: mass, dimensions and c.g. relative distances

Component	Mass [kg]	Dimensions [cm]	C.G. relative distances [m]
Bridge deck + stinger (bs)	1,305		
Bearing central cube (bc)	1,276	7,5x7,5x8,5	
Aluminum cube (ac)	0,349	5x5x5	0,2035 from central cube
Sidebar (bar)	0,32	73,8(l)x0,926(Ø)	
Upper spring (us)	0,014		0,1778 from aluminum cube
Lower spring (ls)	0,004		0,14208 from aluminum cube
Screw ring (sr)	0,024		
Plate (plate)	0,137	7,5x7,5x1	
Plate's bull (bull)	0,042	4 (l)	0,028575 from longitudinal

in Figure 5. The model geometry and dimension are also reported in Figure 5. e isometric view in Figure 4 shows how the deck section is suspended in the center position of the test section by springs vertically connected to the apparatus by hook bolts. The springs used in this experiment have been chosen with a proper stiffness as to be able to demonstrate flutter at a low speed, instead of obtaining a GBB dynamically scaled model. The choice relies in the main purpose of the research that is focused in the validation of the flutter derivatives extraction procedure and their employment for a more consistent simulation model. The mechanical link between the bridge deck section and the spring is obtained by means of a series of rods and aluminum threaded cube as shown in Figure 6. All the mechanical elements contribute to the dynamic behavior of the overall system and therefore are included in the mass and inertial computation. The mass breakdown and their c.g. relative distances are reported in Table 1.

Four load cells (Omega Miniature Low Profile Tension Links LC703-25, with capacity of 11 kgf, 25 lb) are installed in series to each floor anchorage point for measuring purpose. In addition, to guarantee a pure heaving-pitching motion the deck section is restrained in the other degrees of freedom by

an aluminum C-section bar properly milled and greased to minimize friction, as shown in Figure 6. The real time data acquisition system is made of a National Instrument board, for load cells signal-conditioning purpose, connected to a NI-PXI console running a custom made Labview® software, and a Motion Pro-X3 high-speed camera connected to a laptop running its proprietary software, for displacement computation validation, see Figure 7.

A "in-house" procedure has been defined according to the new system identification technique proposed by Chowdhury & Sarkar ([3]). The procedure provides a method to compute each term of the aeroelastic system state matrix and the values of the flutter derivatives. Interested readers are addressed to [3] for more detailed description. The off-line method is based on the analysis of the experimental free vibration time histories coupled with a non-linear regression method. This is an identification procedure used to derive the state matrix of a general dynamical system starting from the experimental time

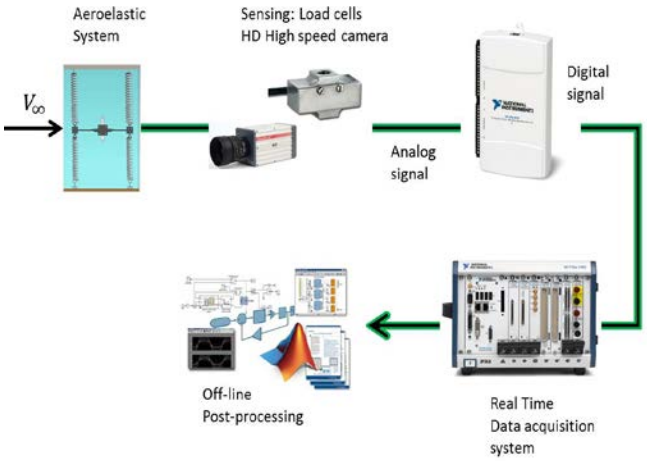

Figure 7 Experiment instrumentation setup.

histories of the states and their derivatives' vectors.

The implemented algorithm is shown in Figure 8 as a block-diagram form [3]. A short description is reported in the following part. Particular attention must be paid to increase accuracy and confidence on the derivative extraction procedure by means of:

- The data acquisition sampling rate of 1000 Hz is reduced, for off-line computation, to 100 Hz to fasten up the iterative algorithm without loss of accuracy.
- Custom-made algorithm is developed for displacement and rotation computation from the load cells voltage time histories. The obtained values are then validated with the high-speed camera output.
- Satisfactory vibration amplitude must be guaranteed, which becomes and issues at high wind speed because of aerodynamic damping.
- An accurate measure of the initial perturbation causing the free decaying motion is required for accuracy and confidence in the ILSM method. In the presented research, the initial conditions are calculated from the application of an impulse in the heave direction h on the deck section.
- The windowing process is crucial to guarantee numerical convergence of the Iterative least Square Method (ILSM). The static variables' interval must be selected of different length and position depending on the analyzed time history to properly calculate the elements of the state matrix [A] from the noisy displacement.

IV. Results

The entire set of flutter derivatives are obtained by experimental procedure diagrammatically described in Figure 8, from either the 1-DOF (torsion) or 2-DOF (coupled) motion systems. The tests are performed at variable wind speed from 0

ILSM pseudo-algorithm

Recast experimental displacement time-histories in vectors $\underline{y}(t_m)$ with $t_m = (m-1)\Delta t$ and $m = 1, 2 \ldots, 2N+2$

Perform zero-phase digital filtering of the signals, here a 3^{rd} order Butterworth, with cutoff frequency $\omega_c = 0.5 \times \pi\, rad/sample$

Computing velocity and acceleration by finite difference

$$\dot{y}(t_{m_k}) = y(t_{m_{k+1}}) - y(t_{m_k})/(t_{m_{k+1}} - t_{m_k})$$
$$\ddot{y}(t_{m_k}) = \dot{y}(t_{m_{k+1}}) - \dot{y}(t_{m_k})/(t_{m_{k+1}} - t_{m_k})$$

Building state vectors $\underline{X}, \underline{\dot{X}}$ employing windowing procedure

For given state vector and state matrix initial conditions $\underline{X_0}$ and $A^0 = (\dot{X}X^T)(XX^T)^{-1}$ perform ILS identification

```
while max(r)>10^-12  % max residual
% simulate new X1
    X1=expm(A*t)*X0;
% Update A matrix
    A(K+1)=(X_dot*X1')/(X*X1)';
% Compute residual
    res(:,:,c)=abs(A(K+1)-A(K));
end
```

when convergence is reached A is identified

Figure 8 Aeroelastic derivative extraction procedure

to 30.6 m/s, with steps related to the wind tunnel fan rpm, as shown in Table 2. In both cases, besides the computation of the dynamical system state matrix and the flutter derivatives, the damped frequency, the damping factor and the natural frequency of the system are experimentally obtained and evaluated, as shown in Figure 9. The system mechanical properties, natural frequency and damping ratio, obtained at zero wind speed are summarized in Table 3.

As far the dynamic test is concerned, it has been accomplished through the following steps:

1) To extract direct derivatives and a 1-DOF pitching motion test, about the center of mass of the section (Δh=0), is performed. A 1-DOF vertical test is not performed because of the excessive damping resulting in unusable time histories.

2) The entire set of flutter derivatives.

The behaviors of the eight flutter derivatives are compared with the theoretical trend obtained from the Theodorsen's theory. The results are shown in function of the reduced velocity, to be properly compared with Scanlan & Tomko ([4]):

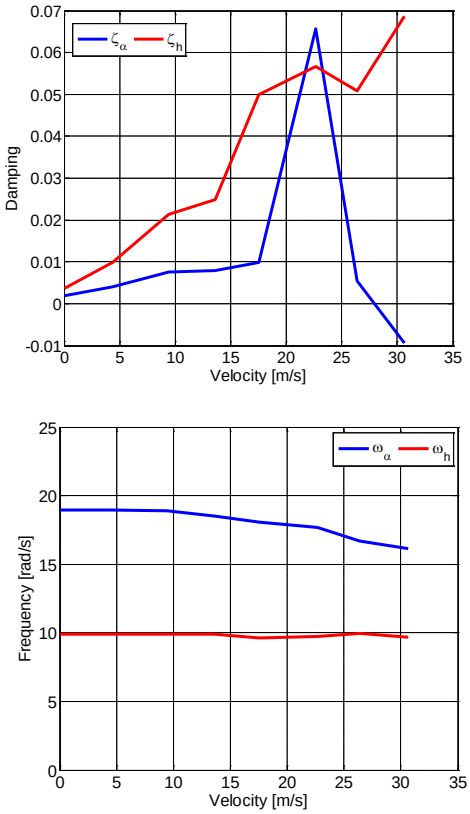

Figure 9 Damping & frequencies as function of wind tunnel speed.

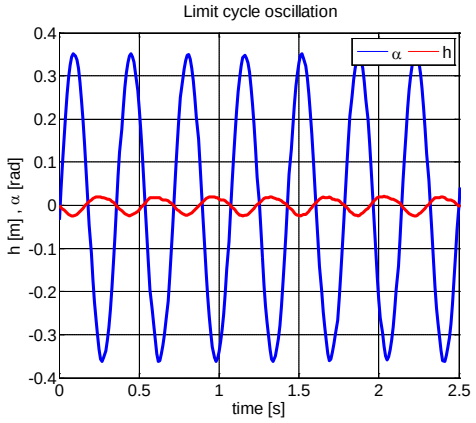

Figure 10 Limit cycle oscillation at flutter speed.

$$U_{red} = \frac{2\pi}{k} = \frac{2\pi V_\infty}{b\omega_f} = \frac{V_\infty}{fb}$$

where f is the oscillation frequency in cycles per second, and all the other parameters have been already defined.

The flutter frequency is used in the formulations of the flutter derivatives. Flutter frequency is extracted

Table 2. Rpm and wind speed experiment steps

rpm	Δp [Pa]	V [m/s]
0	0	0.0
100	11.34	4.4
200	52.9	9.4
300	110.8	13.6
400	182.3	17.5
500	305.4	22.6
600	415,2	26.4
700	557.8	30.6

experimentally: during several tests it is individuated a limit cycle oscillation of the system corresponding to a velocity of $27,9\,m/s$, with a single oscillation frequency.

Figure 10 shows the stable limit cycle with the two motions in plunge and torsion that oscillate at the same frequency (ω_f=17.5 rad/s) . The experimental results, compared with the theory, are shown in the following figures.

In Figure 11, the solid line shows the trend of the flutter derivatives calculated with the Theodorsen's theory, while the dots show the values calculated with 2-DoF system experiment

Table 3. System mechanical properties

$m\,[kg]$	ζ_h	ζ_α	$\omega_h\,[rad/s]$	$\omega_\alpha[rad/s]$
6.605	0.0036	0.0019	9.89	18.96

and the squares, only available for A_2^*, A_3^*, are the values obtained with the 1-DOF in torsion experiment. It is relevant from the representation of the flutter derivatives that their correspondence to the theoretical values is quite good up to the flutter speed. However, even if the trend is preserved, the values' distribution is less precise for U_red above the flutter condition, either in case of 2-DOF plunging and pitching or 1-DOF in pure torsion. Since flutter derivatives are a result of a linear description any non-linearity, due for example to oscillations induced by vortex shedding or post-critical conditions, are not representable by the Theodorsen's formulation which is strictly linear and based on small perturbation approximation. Flutter derivatives H_3^*, H_4^* and A_3^*, A_4^* are referred to the aerodynamic stiffness of the system. Flutter derivatives H_1^*, H_2^* and A_1^*, A_2^* instead are referred to the aerodynamic damping that induce a damped or undamped behavior in the fluid-structures interaction. The values of the derivative H_1^* are always negative and this is relative to a damped behavior of the section in plunge motion (damping due to the actions of the airflow on the structure when the deck section oscillates in plunge). Considering figure relative to the derivative A_2^* an inversion of the curve sign at high velocity is noted; this derivative is relative to the torsional stability of the section that in this case presents a reduction in torsional stability with the crossing of the zero axis at high velocity, approximately at 30 m/s, which is a characteristics of a post- flutter condition. Consistency is found among 2-DOF and 1-DOF data results for A_2^*,A_3^* derivatives at small values of reduced velocity. In both cases, there are some discrepancies at higher velocities, approaching the velocity of flutter and the unstable region. The errors between experiment and theoretical modeling in the flutter derivatives is attributed to measurement errors due to the fan of the wind tunnel, since it was difficult to keep a constant velocity during all tests, as the laboratory room was quite small and flow non-uniformity affected the measurement. This variability is acceptable (1 – 1.5 m/s) but may influence the results especially at high velocity, where we noted larger discrepancies. This problem might be associated with the cavitation of the fan blades. The motor dispose a larger quantity of fluid with respect to the real amount and this can cause a waste of power and non-constant velocity in the tunnel.

In order to obtain a validation of the results, a Simulink model was implemented and will be used for future aeroelastic control applications. Using the Simulink model is possible to verify the experimental results relative to the flutter derivatives, introducing them in the equations of motion. The model is run to simulate the dynamic behavior of the bridge deck section at different velocity, to compute the flutter condition and to verify the correct motion of the section at each velocity. Some simulations are performed from V_∞=0 m/s to V_∞=30 m/s with steps of 5 m/s, and fitting in proximity of the flutter occurrence. When the velocity is increased, we note the more dumped behavior of the section, up to the limit cycle condition (individuated at V_∞=27,5 m/s), up to the divergent motion above the flutter velocity.

Flutter condition V=27,5 m/s is almost the same of the experimentally determined value V_∞=27,9 m/s. This is a minimal discrepancy between real and simulated model, which confirm the efficacy and consistency of the employed methodologies. Some results are shown in the following figure when it is possible to see the different dynamic behavior in function of the velocity.

V. Conclusions

Large Numerical and experimental comparison of flutter derivatives for a 2D heaving-pitching apparatus representative of long span structures (bridges or wings) is reported in this paper. The experimental derivatives were extracted following an identification technique based on free vibration time histories and the non-linear regression method Iterative Least Square Method (ILSM). The method was applied to a typical bridge section with stiffness characteristics calibrated in order to demonstrate flutter in the low speed wind tunnel performed tests. The flutter derivatives are experimentally obtained either from the 1-DOF torsion test or 2-DOF plunging and pitching coupled motion test. The numerical flutter derivatives are obtained by the application of Theodorsen's thin airfoil formulation in unsteady motion. The presented results demonstrated a quite good correspondence between theoretical and experimental trends at the pre-critical and critical condition for both the 2-DOF or 1-DOF test cases. Due to nonlinearities existing in the post-critical regime, the proposed analytical formulation is not capable to give satisfactory results. A simulation model in MATLAB/Simulink® environment was finally developed and validated by experimental pre-flutter and flutter results. The accuracy in the prediction of the flutter speed of the model implemented using experimentally extracted flutter derivatives is found to be higher than when using solely a theoretical formulation. This is particularly important when studying the flexible high-aspect-ratio wing such as HALE wing or flexible morphing aircraft configuration. The identification of aeroelastic derivatives is a basic step used in the simulation of critical flight operations to assess potentially dangerous conditions. Future investigation will be carried out using flexible wing model with direct measurements from wind tunnel testing. The model will take into consideration also new or future structural configurations such as oriented stiffened structures with specific couplings that modify aeroelastic behavior in critical or post-critical flight conditions.

.

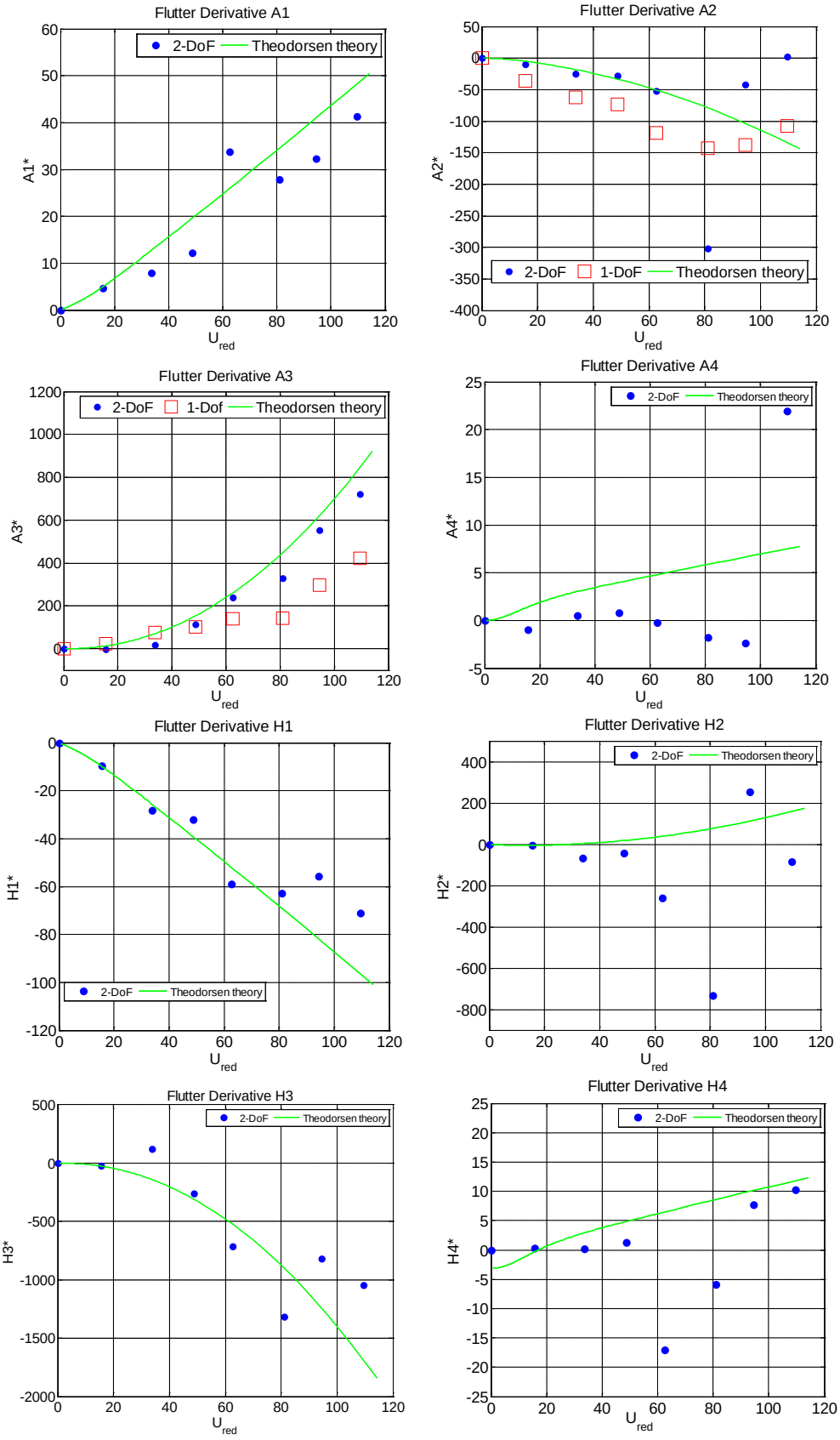

Figure 11 Experimental Flutter derivatives vs Theodorsen's analytical formulation.

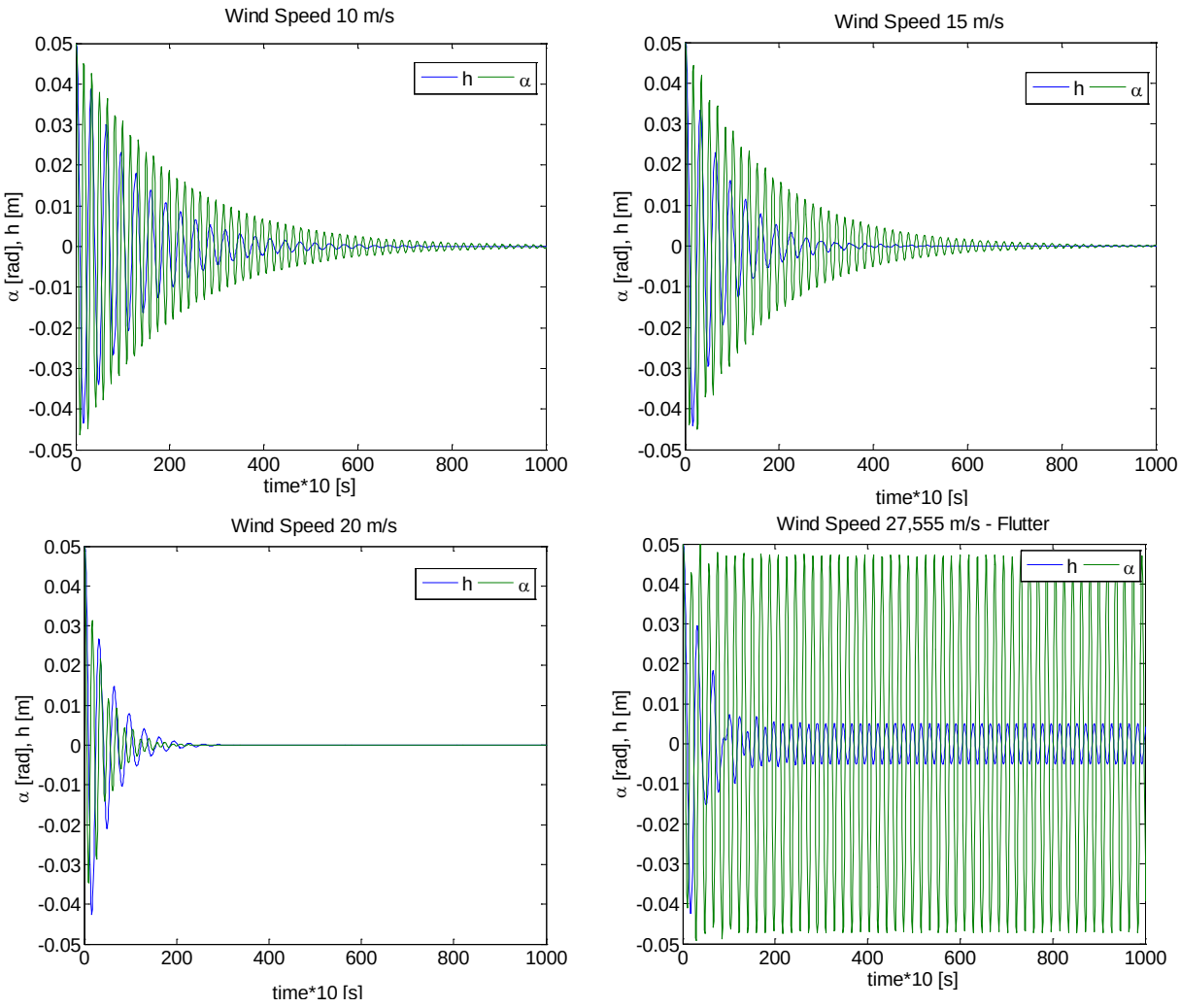

Figure 12 Simulation model results, based on the extracted flutter derivatives.

ACKNOWLEDGMENT

Special thanks to the Clarkson Universiy staff members for assisting with the experimental activity.

REFERENCES

[1] Wright, J. R. & Cooper, J. E., 2007. Introduction to Aircraft Aeroelasticity and Loads. J. Wiley & Sons: s.n

[2] Ashley, H., Bisplinghoff, R. L. & Halfman, R. L., 1996. Aeroelasticity. New York: Dover .

[3] Chowdhury, A. & Sarkar, P., 2003. A new technique for identification of eighteen flutter derivatives using a three-degrees-of-freedom section model. Engineering Structures, Volume 25, pp. 1763-1772.

[4] Scanlan, R. H. & Tomko, J. J., 1971. Airfoil and Bridge Deck Flutter Derivatives. Journal of the Engineering Mechanics Division Proceeding of the American Society of Civil Engineering.

[5] Scanlan, R. H. J. J., 1971. Airfoil and bridge deck flutter derivatives. ASCE Journal of the Engineering Mechanics Division, Volume 97, pp. 1717-1737.

[6] Scanlan, R. H., 1997. Some observations on the state of bluff-body aeroelasticity. Journal of Wind Engineering and Industrial Aerodynamics, Volume 69-71, pp. 77-93.

[7] Cestino, E., Frulla, G., Perotto, E. & Marzocca, P., 2011. Theoretical and Experimental Flutter Predictions in High Aspect Ratio Composite Wings.. SAE INTERNATIONAL JOURNAL OF AEROSPACE, 4(2), pp. 1365-1372.

[8] Borello, F., Cestino, E. & Frulla, G., 2010. Structural Uncertainty Effect on Classical Wing Flutter Characteristics. JOURNAL OF AEROSPACE ENGINEERING, 23(4), pp. 327-338.

[9] Ming G., R. Z. H. X., 2000. Identification of futter derivatives of bridge decks. Journal of Wind Engineering and Industrial Aerodynamics, Volume 84, pp. 151-162.

[10] Chowdhury A.G., S. P., 2003. A new technique for identification of eighteen flutter derivatives using a three-degree-of-freedom section model. Engineering Structures, Volume 25, p. 1763–1772.

[11] Arena, A., Lacarbonara, W. & Marzocca, P., 2016. Post-Critical Behavior of Suspension Bridges under Nonlinear Aerodynamic Loading. Journal of Computational and Nonlinear Dynamics, 11(1).

[12] Arena, A., Lacarbonara, W., Marzocca, P. & Valentine, D., 2014. Aeroelastic behavior of long-span suspension bridges under arbitrary wind profiles. Journal of Fluids and Structures, 50(10), pp. 105-119.

[13] Ebrahimnejad, L., Janoyan, K., Valentine, D. & Marzocca, P., 2014. Investigations of the Aerodynamic Analysis of Super Long-Span Bridges by Using ERA Based Reduced Order Models. Journal of Bridge Engineering, 19(9).

[14] Farsani, H. et al., 2014. Indicial Functions in the Aeroelasticity of Bridge Decks. Journal of Fluids and Structures, Volume 48, pp. 203-215.

[15] Bruni, C., Cestino, E., Frulla, G. & Marzocca, P., 2015. Nonlinear Slender Beam-Wise Schemes for Structural Behavior of Flexible UAS Wings. SAE Technical Paper.
[16] Cestino, E., Frulla, G., Perotto, E. & Marzocca, P., 2014. Experimental Slender Wing Model Design by the Application of Aeroelastic Scaling Laws. JOURNAL OF AEROSPACE ENGINEERING, 27(1), pp. 112-120.
[17] Frulla, G. & Cestino, E., 2014. Analysis of slender thin-walled anisotropic box-beams including local stiffness and coupling effects. AIRCRAFT ENGINEERING AND AEROSPACE TECHNOLOGY, 86(4), pp. 345-355.
[18] Bruni C.; Cestino E.; Frulla G.; Gibert J.; Marzocca P. (2015). A Multi-objective Nonlinear Piezoaeroelastic Wing Solution for Energy Harvesting and Load Alleviation: Modeling and Simulation. 56th AIAA/ASCE/AHS/ASC Structures, Structural Dynamics, and Materials Conference. Florida (USA), 5-9 January 2015.
[19] Bruni C.; Gibert, J.; Frulla G.; Cestino E.; Marzocca, P. (2017). Energy harvesting from aeroelastic vibrations induced by discrete gust loads. JOURNAL OF INTELLIGENT MATERIAL SYSTEMS AND STRUCTURES. - ISSN 1045-389X. - 28:1(2017), pp. 47-62.
[20] Bruni C., Cestino E. , Frulla G., Marzocca P., Gibert J. and D'Onghia N. (2017). Practical considerations for the design of an aeroelastic energy harvester. International Forum on Aeroelasticity and Structural Dynamics. IFASD 2017. 25-28 June 2017, Como - Italy.
[21] Bruni C., Cestino E., Frulla G.(2016). Parametric analysis of a fluttering piezoelectric wing . AIRCRAFT ENGINEERING AND AEROSPACE TECHNOLOGY. - ISSN 1748-8842. - 88:3(2016), pp. 382-388.
[22] Cestino E.; Frulla G.; Marzocca P . (2013).A Reduced Order Model for the Aeroelastic Analysis of Flexible Wings. DOI:10.4271/2013-01-2158. In SAE INTERNATIONAL JOURNAL OF AEROSPACE - ISSN:1946-3855 vol. 6 (2), 2013.
[23] Baghdasaryan, G.Y.; Mikilyan, M.A.; Saghoyan, R.O.; Cestino, E.; Frulla, G.; Marzocca, P. (2015). Nonlinear LCO “amplitude-Frequency”Characteristics for Plates Fluttering at Supersonic Speeds. DOI:10.1016/j.ijnonlinmec.2015.06.014. 2015, pp.51-60. In INTERNATIONAL JOURNAL OF NON-LINEAR MECHANICS - ISSN:0020-7462.
[24] Bruni, Claudia; Cestino, Enrico; Frulla, Giacomo; Marzocca, Piergiovanni (2015) Nonlinear Slender Beam-Wise Schemes for Structural Behavior of Flexible UAS Wings, In: SAE TECHNICAL PAPER, ISSN: 0148-7191, 2015.
[25] Seber, G. A. F. & Wild, C. J., 2003. Nonlinear Regression. s.l.:Wiley-Interscience, J. Wiley & Sons
[26] Cassaro, M. et al., 2013. ℒ1 Adaptive Flutter Suppression Control Strategy for Highly Flexible Structure. SAE INTERNATIONAL JOURNAL OF AEROSPACE, 6(2), pp. 693-702.
[27] Theodorsen, T., 1935. General Theory of Aerodynamic Instability and the Mechanism of Flutter, s.l.: NACA TR 496.
[28] Scanlan, R. H., Jones, N. P. & Singh, L., 1997. Inter-relations among flutter derivatives. Journal of Wind Engineering and Industrial Aerodynamics, Volume 69-71, pp. 829-837..